RSC Advances

PAPER

View Article Online
View Journal | View Issue

Cite this: *RSC Adv.*, 2026, **16**, 24838

Hyaluronic acid-modified Fe-based metal–organic framework loaded with cisplatin for targeted lung cancer therapy

Ammar Saleem,[a] Komal Zaman Khan,[a] Eman Fayad,[b] Aurang Zaib,[a] Ghazanfar Abbas,[a] Dalal Nasser Binjawhar,[c] Ali Junaid,[d] Muhammad Naeem Ashiq,[d] Zahid Shafiq *[d] and Hua Li Qin *[a]

Lung cancer is still the most common cause of cancer fatalities around the world. To address these issues, we fabricated a cisplatin-containing hyaluronic acid-modified Fe-MOF that was designed to release drugs in response to changes in pH and actively target lung cancer cells. The incorporation of HA, which specifically binds to CD44 receptors that are overexpressed on the surface of lung cancer cells, improves cellular uptake and therapeutic effectiveness. The pH-dependent behavior is confirmed by *in vitro* drug release experiments, demonstrating little cisplatin release at physiological pH and enhanced release within the acidic tumor microenvironment. Cytotoxicity studies showed that HA/Fe-MOF/CP is more effective against A549 lung cancer cells than free cisplatin (82.72% inhibition at 50 μM and IC_{50} = 17.3 ± 0.5 μM). HA/Fe-MOF/CP showed less toxicity to normal BEAS-2B cells (85.34% viability and IC_{50} > 40 μM), while free cisplatin showed more toxicity to BEAS-2B cells (23.16% inhibition and IC_{50} > 40 μM). The uncoated Fe-MOF/CP inhibited A549 cells by 76.42% (IC_{50} = 22.4 ± 0.3 μM), which indicates a moderate level of effectiveness. Fe-MOF has been altered a significant effect on cancer cells (60.41% inhibition and IC_{50} = 35.6 ± 0.5 μM) and worked well with BEAS-2B cells (89.31% viability).

Received 28th January 2026
Accepted 15th April 2026

DOI: 10.1039/d6ra00754f

rsc.li/rsc-advances

1. Introduction

Cancer is still one of the most significant health problems globally, killing millions of people every year.[1] Lung cancer is among the most prevalent and deadly cancers and a leading cause of death worldwide.[2] Smoking is the primary cause of cancer fatalities in the US, accounting for around 85% of all lung cancer cases.[3] Lung cancer cases have been increasing significantly, and estimations indicate that the number of lung cancer deaths will continue to rise until 2030.[4] The prognosis for lung cancer is poor; in the advanced stages of the disease, the five-year survival rate remains below 20%.[5] Chemotherapy has been a key part of treatment, and it is often used with surgery and radiation therapy.[6] However, systemic toxicity, poor pharmacokinetics, multidrug resistance, and insufficient tumour targeting hinder the development of therapies that improve long-term survival.[7] Chemotherapy cannot differentiate between healthy and cancerous cells in advanced-stage lung cancer, which is why these problems are difficult to address.[8] Bone marrow suppression, liver and kidney damage, nausea, and fatigue are some of the serious side effects that may arise from such failures.[9]

To address these challenges, recent improvements in drug delivery systems (DDS) have focused on making therapeutic agents more bioavailable, more specific to their targets, and easier to control when they are released.[10] Metal–organic frameworks (MOFs) and other nanocarriers have become promising platforms for the prolonged and regulated administration of drugs due to their unique advantages, including biodegradability, large surface area, and adjustable pore size.[11] Iron based MOFs (Fe-MOFs) that are safe for the body and work well with living organisms, like have shown a lot of promise for delivering drugs, especially for treating cancer.[12] Iron-based MOFs (Fe-MOFs) are great for targeted cancer therapy because they can load extensive amounts of chemotherapy drugs and remain stable under both aqueous conditions and in organic solvents.[13] Adding different targeting ligands to these materials can render them more specific to cancer cells.[14]

We are working on a new system for targeted drug delivery called HA/Fe-MOF/CP. This system treats lung cancer with an Fe-MOF that has been modified with hyaluronic acid (HA) and filled with cisplatin (CP). Hyaluronic acid (HA) is a naturally occurring anionic polysaccharide composed of repeating

[a]*School of Chemistry, Chemical Engineering and Life Sciences, Wuhan University of Technology, Wuhan 430070, China. E-mail: qinhuali@whut.edu.cn*
[b]*Department of Biotechnology, College of Science, Taif University, P.O. Box 11099, Taif 21944, Saudi Arabia*
[c]*Department of Chemistry, College of Science, Princess Nourah Bint Abdulrahman University, P.O. Box 84428, Riyadh 11671, Saudi Arabia*
[d]*Institute of Chemical Sciences, Bahauddin Zakariya University, Multan 60800, Pakistan. E-mail: zahidshafiq@bzu.edu.pk*

disaccharide units of D-glucuronic acid and *N*-acetyl-D-glucosamine linked *via* alternating β(1→3) and β(1→4) glycosidic bonds. Owing to its biocompatibility and ability to specifically bind CD44 receptors that are overexpressed on lung cancer cell surfaces, HA plays a crucial role within the tumor microenvironment (TME).[15,16] In this study, HA was utilized to functionalize iron-based metal–organic frameworks (Fe-MOFs) to enhance tumor selectivity and promote receptor-mediated cellular uptake. The HA used ($M_w \approx 120$ kDa, intrinsic viscosity 3.8 dL g^{-1}, as determined by gel permeation chromatography and Ubbelohde viscometry) also improved the hydrophilicity and colloidal stability of the Fe-MOF.[17] This modification enabled controlled, pH-responsive release of cisplatin (CP) in the acidic TME, thereby enhancing therapeutic efficacy while minimizing systemic toxicity.[18] Numerous systems have been developed for targeted drug delivery using metal–organic frameworks (MOFs), including those modified with hyaluronic acid (HA) to target CD44 receptors. While many of these systems utilize MOFs for drug encapsulation, our work stands out by integrating multiple features into a single nanoplatform. Specifically, we have designed a system that combines pH-responsive drug release, HA-mediated CD44 targeting, and enhanced biocompatibility, which results in reduced off-target toxicity and improved tumor-specific drug delivery.

The most commonly used drug for lung cancer treatment is cisplatin, which works by attaching to the DNA of cancer cells, reducing growth and killing cells.[19,20] But its clinical efficacy is constrained by systemic toxicity, inadequate solubility, and a lack of selective targeting of cancer cells.[21] To overcome these problems and make treatment more accurate, we modified cisplatin in HA-functionalized Fe-MOFs. The pH-sensitive properties of Fe-MOFs enable controlled release of cisplatin in the acidic tumor microenvironment, thereby improving therapeutic efficacy and minimizing the adverse effects associated with conventional chemotherapy.[22] J.-J. Shen *et al.* developed a (Luteolin + Matrine) NH_2-MIL-101(Fe)@GO system with 9.8% and 14.1% drug loading efficiencies, showing pH-sensitive release: 54.8% and 60.8% at pH 5, and 17.8% and 58.3% at pH 7.4, respectively.[23] P. Raju *et al.* synthesized a FU@Eu-MOF nanocomposite with 22.15 wt% loading capacity, from which drug release was limited to 15.4% at pH 7.4 but increased to 53.6% (pH 6) and 85.3% (pH 5).[24] A. Ahmed *et al.* designed a PEG-FA-NH_2-Fe-BDC for doxorubicin delivery with 97% encapsulation efficiency and 14.5 wt% encapsulation capacity, while the pH/US dual responsive DOX release efficiency was 44.4% at pH 7.4, increasing to 90% at pH 5.3 with US, and 36% at pH 7.4, increasing to 70.2% at pH 5.3 without US.[25] Yang *et al.* designed a MIL-100@Apa@MPN with a drug-loading and encapsulation efficiency of 28.33% and 85.01%, respectively, from which drug release was limited to 42.31% at pH 7.4 and increased to 73.72% at acidic pH 5.[26]

This study reports the design and synthesis of a hyaluronic acid-functionalized iron-based metal–organic framework loaded with cisplatin (HA/Fe-MOF/CP) for targeted lung cancer therapy. The novelty of this study lies in the optimized combination of CD44-targeting, pH-responsive drug release, and selective cytotoxicity toward lung cancer cells. The hypothesis of this work is that HA modification of Fe-MOF enhances tumor-specific targeting and pH-responsive release of cisplatin, thereby improving its antitumor efficacy while minimizing systemic toxicity. Hyaluronic acid (HA), a naturally occurring polysaccharide with a high affinity for CD44 receptors overexpressed on lung cancer cells, was employed to confer selective targeting and improved biocompatibility. The Fe-MOF core serves as a stable and efficient nanocarrier, while HA functionalization increases hydrophilicity and bioavailability, enabling controlled, pH-sensitive drug release within the tumor microenvironment. HA/Fe-MOF/CP effectively mitigates the limitations of free cisplatin, including poor pharmacokinetics, high systemic toxicity, and non-specific biodistribution, by facilitating tumor-selective accumulation. *In vitro* cytotoxicity assays demonstrated that HA/Fe-MOF/CP exhibited markedly lower toxicity toward BEAS-2B normal lung epithelial cells (17.23% inhibition; 85.34% viability; IC_{50} > 40 μM) while maintaining potent anticancer activity against A549 lung cancer cells (82.72% inhibition; $IC_{50} = 17.3 \pm 0.5$ μM). In contrast, free cisplatin caused higher toxicity to BEAS-2B cells (23.16% inhibition; 76.23% viability; IC_{50} > 40 μM). HA/Fe-MOF/CP is thus a promising nanoplatform for the safe and efficient delivery of cisplatin, offering enhanced tumor selectivity, controlled release, and reduced off-target toxicity for lung cancer treatment.

2. Experimental section

2.1 Materials and methods

Ferric chloride hexahydrate ($FeCl_3 \cdot 6H_2O$, 98%), hyaluronic acid ($(C_{14}H_{21}NO_{11})_n$, 85%), benzene-1,3,5-tricarboxylic acid (BTC, 95%), parabenzoquinone ($C_6H_4O_2$, 99%), and absolute ethanol were purchased from Sigma Aldrich. Hyaluronic acid (sodium hyaluronate; $(C_{14}H_{20}NO_{11}Na)_n$, CAS no. 9067-32-7), with a molecular weight of 1.0–1.8 MDa and purity ≥98%, was obtained from Sigma Aldrich. These chemicals were all utilized as received, without additional purification.

2.2 Characterization

Powder X-ray diffraction (PXRD) patterns were recorded on a Panalytical Empyrean diffractometer (Malvern Panalytical, Spectris Plc, England) using BBHD Cu-Kα radiation ($\lambda = 1.5406$ Å). Samples were ground into fine powder, placed on a glass sample holder, and scanned in the 2θ range of 5° to 80° with a step size of 0.01° and a scanning speed of 10° min^{-1} at 40 kV and 40 mA. Fourier-transform infrared (FTIR) spectra were recorded on a Thermo Fisher Scientific NICOLET iS50 spectrometer (Thermo Fisher Scientific, Waltham, MA, USA) in attenuated total reflectance (ATR) mode over the wavenumber range of 400–4000 cm^{-1} with a resolution of 4 cm^{-1} and 64 scans. Sample preparation for solid powder: 1 mg of the sample and 100 mg of potassium bromide were mixed thoroughly and ground into a powder. A tablet press was then used to compress the powder into a transparent tablet for testing. The surface morphology of the samples was examined using field-emission scanning electron microscopy (FE-SEM) on a Carl Zeiss ULTRA

55 (Carl Zeiss AG, Oberkochen, Germany). The surface morphology and elemental composition of the samples were examined using field-emission scanning electron microscopy (FE-SEM) on a ZEISS Sigma 300 (Carl Zeiss AG, Oberkochen, Germany), equipped with an energy-dispersive X-ray spectrometer (EDX, Oxford Instruments, Abingdon, UK). Powder samples were dispersed on carbon tape mounted on aluminum stubs and sputter-coated with gold for 60 s prior to imaging at an accelerating voltage of 5–15 kV. High-resolution transmission electron microscopy (HR-TEM) images were obtained using a JEOL JEM-F200 microscope (JEOL Ltd, Tokyo, Japan) operated at 200 kV. Samples were dispersed in water by sonication for 10 min, and a drop of the suspension was placed on a carbon-coated copper grid and air-dried at room temperature before analysis. X-ray photoelectron spectroscopy (XPS) was carried out using a Thermo Fisher Scientific K-Alpha spectrometer (Thermo Fisher Scientific, Waltham, MA, USA) with monochromatic Al-Kα radiation (1486.6 eV). Survey and high-resolution spectra were collected at a pass energy of 50 eV. Powder samples were pressed onto indium foil for analysis, and charge neutralization was applied. Zeta potential measurements were performed on a Malvern Panalytical Zetasizer Nano S90 (Malvern Panalytical Ltd, Malvern, UK). Samples were dispersed in deionized water (concentration ~0.1 mg mL^{-1}), sonicated for 5 min, and measured at 25 °C using disposable folded capillary cells. Three measurements were averaged for each sample. UV-Vis absorption spectra for drug loading, release, and TMB oxidation studies were acquired using a Shimadzu UV-1800 spectrophotometer (Shimadzu Corporation, Kyoto, Japan) in the wavelength range of 200–800 nm using quartz cuvettes with a path length of 1 cm. Samples were appropriately diluted in the respective medium, and baseline correction was performed with the blank medium.

2.3 Synthesis of Fe-MOF

$FeCl_3 \cdot 6H_2O$ (20 mmol) and 1,3,5-benzene tricarboxylic acid (BTC) (20 mmol) were dissolved in 70 mL of ethanol (C_2H_5OH) to create Fe (BTC) MOF. Parabenzoquinone (10 mmol) was then added and the mixture was stirred for 30 minutes to ensure a homogeneous solution. The resulting solution was then transferred to a 100 mL stainless-steel autoclave lined with Teflon and heated at 120 °C for 24 hours. After the reaction period, the mixture was allowed to cool to room temperature. The solid product was filtered, and the precipitate was collected. The product was then washed with 3 × 20 mL of ethanol and dried for 12 hours at 60 °C in a vacuum oven. The samples collected after drying were designated as Fe-MOF (Scheme 1).

2.4 Synthesis of Fe-MOF/cisplatin (CP)

Cisplatin loading into the Fe-based MOF was carried out by immersing 0.1 g of Fe-MOF and 0.1 g of cisplatin in 20 mL of deionized water, followed by sonication for 30 minutes. The mixture was then stirred in a tightly sealed Teflon container for 36–48 hours. Afterward, the solution was centrifuged to remove the solvent, and the resulting product was air-dried (Scheme 2).

The following equation is used to determine the loading efficiency of the drug:

$$\text{Encapsulation efficiency } (\%) = \frac{\text{Mass of incapsulated drug}}{\text{Mass of total drug added}} \times 100$$

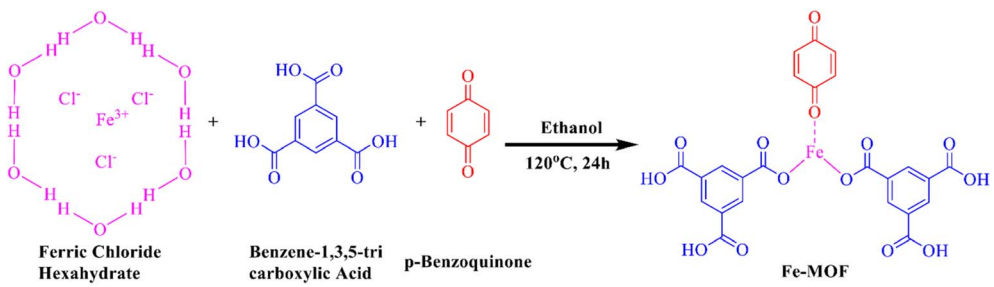

Scheme 1 Reaction scheme for the synthesis of Fe-MOF.

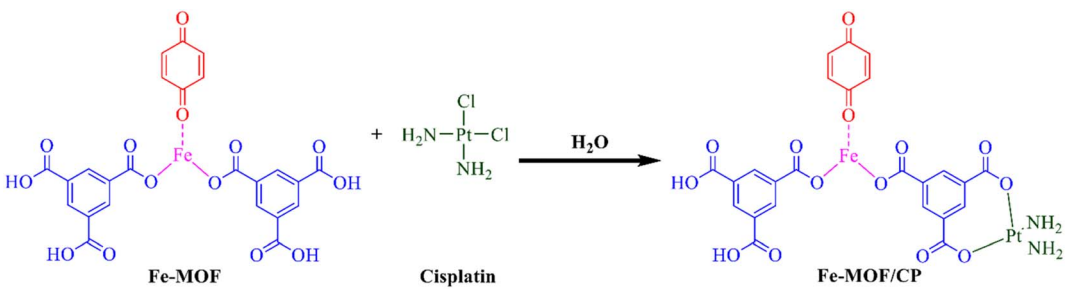

Scheme 2 Reaction scheme for the loading of Fe-MOF/CP.

where C_{en} and C_{in} represent the amount of encapsulated cisplatin over its input quantity, respectively, during the process (mg).

2.5 Synthesis of hyaluronic acid (HA) functionalized Fe-MOF

Stock solutions of ultrapure water (10 mL) and ethanol (20 mL) were combined and subjected to sonication for one hour. Subsequently, Fe-MOF (3 mg mL^{-1}) and hyaluronic acid (HA) (12 mg mL^{-1}) were added dropwise in sequence. The mixture was then exposed to ultrasound for 4 hours and stirred for 20 hours at 25 °C with a speed of 800 rpm. The resulting HA-functionalized Fe-MOF was washed three times with ultrapure water, dispersed in ethanol, and collected after being air-dried (Scheme 3).

2.6 Synthesis of HA/Fe-MOF/CP

Stock solutions of alkaline cisplatin (1 mg mL^{-1}) (30 mL) and ethanol (EA) (20 mL) were mixed and subjected to sonication for one hour. Fe-MOF (3 mg mL^{-1}) and hyaluronic acid (HA) (12 mg mL^{-1}) were then added dropwise in sequence. The mixture was treated with ultrasound for 4 hours and stirred for 20 hours at 25 °C with a speed of 800 rpm. The resulting cisplatin-loaded HA-functionalized Fe-MOF was washed three times with ultrapure water, dispersed in ethanol, and collected after being air-dried (Scheme 4).

2.7 Synthesis scheme

See Scheme 5.

2.8 Drug delivery

For drug loading, the Fe-MOF nanocarriers were activated under vacuum at 100 °C for 24 hours to eliminate any coordinated solvent molecules residing in the pores. Briefly, 100 mg of Fe-MOF was suspended in a 30 mL solution of cisplatin (1000 ppm) in ethanol. The solution was placed on a shaker at room temperature for 48 hours. Subsequently, the cisplatin-loaded HA-functionalized Fe-MOFs were isolated *via* centrifugation, and the supernatant was examined to quantify the residual drug. The drug loading capacity (DLC) and drug loading efficiency (DLE) of the nanocarriers were determined using a calibration curve of cisplatin in ethanol ($\lambda_{max} = 270$ nm) based on the following formulae.

$$\text{DLE (wt\%)} = \frac{\text{weight of loaded CP}}{\text{intial weight of CP}} \times 100$$

$$\text{DLC (wt\%)} = \frac{\text{amount of drug loaded CP (mg)}}{\text{total weight of carrier}} \times 100$$

2.9 Drug release

The pH-responsive drug release from the samples was assessed in PBS solutions mimicking both the tumor microenvironment (TME, pH 5) and physiological conditions (pH 7.4). Briefly, 60 mg of cisplatin-loaded HA/Fe-MOF was dispersed in a dialysis bag (3.5 kDa MWCO) containing a small amount of PBS. The dialysis bag carrying the drug-loaded nanocarriers was then placed in a beaker with 60 mL of PBS (pH 5 and 7.4). The drug release was carried out through dialysis at 37 °C under continuous stirring. At predetermined intervals, 2 mL of the

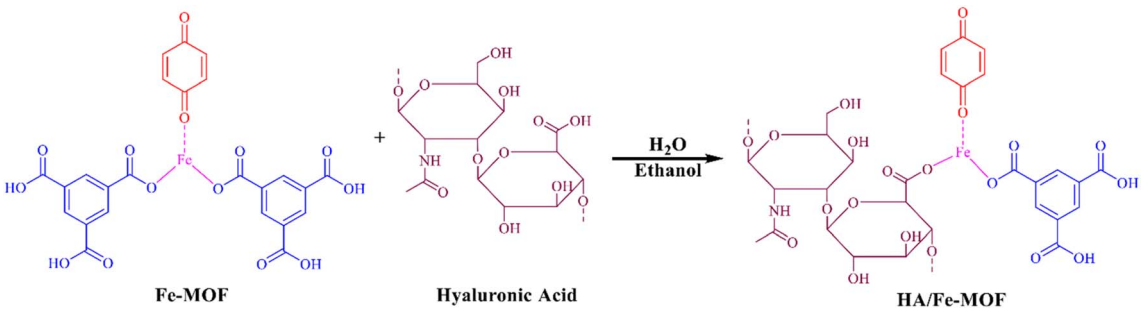

Scheme 3 Reaction scheme for the synthesis of HA/Fe-MOF.

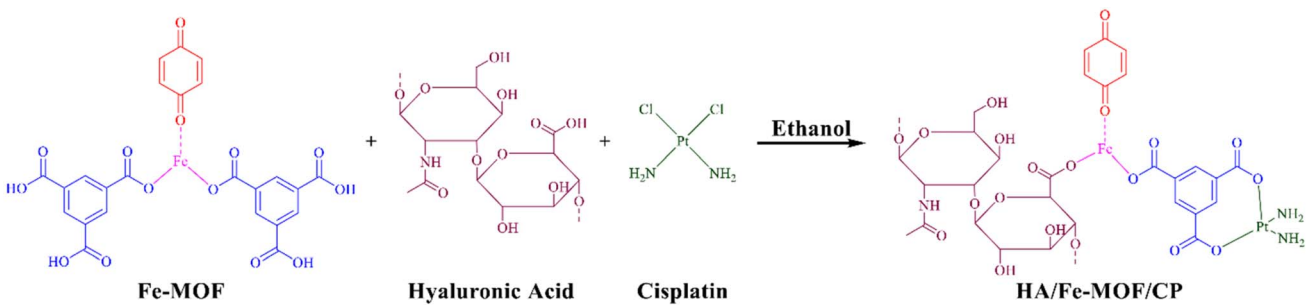

Scheme 4 Reaction scheme for the synthesis of HA/Fe-MOF/CP.

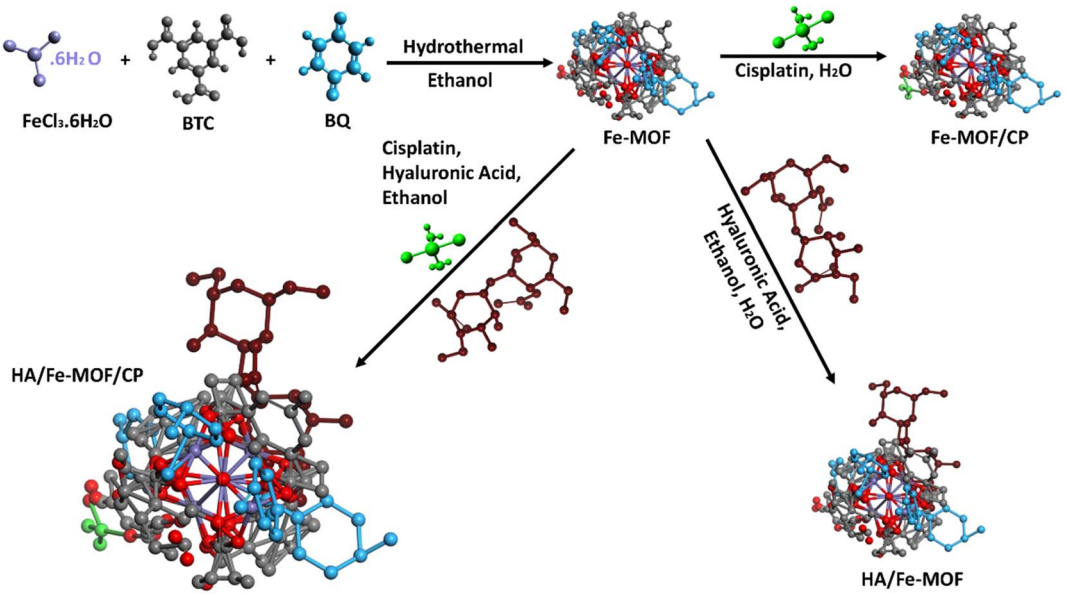

Scheme 5 Synthesis scheme of Fe-MOF, Fe-MOF/CP, HA/Fe-MOF, and HA/Fe-MOF/CP.

dialysate solution was withdrawn and exchanged with an equal volume of fresh PBS to keep the total volume constant. The withdrawn samples were investigated using a UV-vis spectrophotometer, and the concentration of the released cisplatin was determined according to the calibration curve of cisplatin in PBS (λ_{max} = 270 nm). The experiments were performed in duplicate, and the results were averaged and plotted. The following equations were used to calculate the cumulative cisplatin release percentage:

$$\text{Drug release (cumulative\%)} = \frac{Rt}{Rf} \times 100$$

where R_t denotes the cisplatin concentration released at time t, and R_f represents the total amount of cisplatin loaded on the HA/Fe-MOF nanocarriers.

2.10 *In vitro* pharmacokinetics study of released cisplatin

To assess and define the kinetics and mechanism governing the cisplatin release, zero-order (eqn (1)), first-order (eqn (2)), Higuchi (eqn (3)), and Korsmeyer–Peppas (eqn (4)) kinetic models were applied to the *in vitro* cisplatin release data (Fig. S1–S4). The correlation coefficient (R^2) for each equation was calculated to evaluate whether the experimental results fit the respective model. Additionally, the mechanism of drug release was determined by calculating the diffusional exponent "n". The value of "n" helps identify the release mechanism: a value of 1.0 corresponds to Case II transport, 0.45–1.0 indicates non-Fickian diffusion, and a value ≤ 0.45 suggests Fickian diffusion.

$$Q = k_0 t \quad (1)$$

$$\text{Ln } Q = \ln Q_0 - k_1 t \quad (2)$$

$$Q = k_H t^{1/2} \quad (3)$$

$$\text{Ln } Q = n\text{Ln } t + \text{Ln } k_p \quad (4)$$

In eqn (1)–(4), k_0, k_1, k_H, and k_p display the rate constant of the zero-order, first-order, Higuchi, and Korsmeyer-Peppas kinetic models, respectively, and Q is the amount of released drug.[27]

2.11 Cell culture

The cells were grown in RPMI-1640 medium augmented with 1% Pen-strep (100 IU mL^{-1} penicillin and 100 μg mL^{-1} streptomycin), 10% Hi-FBS, and 2 mM L-glutamine in a humidified incubator at 37 °C with 5% CO_2. Cytotoxicity assays were completed to assess the anticancer potential of the HA/Fe-MOF/cisplatin fabricated. A549 lung cancer cells were treated with varying concentrations of HA/Fe-MOF/Cisplatin, showing significant inhibition, with 82.72% inhibition at 40 μM and an IC_{50} of 17.3 ± 0.5 μM, compared to free cisplatin, which exhibited 72.91% inhibition at 40 μM with an IC_{50} of 23.2 ± 0.7 μM (Table 1). BEAS-2B normal lung epithelial cells were also treated, showing 17.23% inhibition (IC_{50} > 40 μM) at 40 μM for HA/Fe-MOF/CP, indicating selective toxicity toward cancer cells, compared to cisplatin, which showed 23.16% inhibition at 40 μM with an IC_{50} of >40 μM.

2.12 Cell cytotoxicity assay

In vitro cytotoxicity of cisplatin, Fe-MOF, Fe-MOF/Cisplatin, HA/Fe-MOF, and HA/Fe-MOF/CP was evaluated by the MTT assay. Briefly, A549 lung cancer cells and BEAS-2B normal lung epithelial cells were seeded in a 96-well plate at a density of 1 × 10^4 cells per well and incubated in a CO_2 incubator for 24 h at 37 °C. A549 lung cancer cells and BEAS-2B normal lung epithelial cells were obtained from the Cell Bank of the Chinese Academy of Sciences (Shanghai, China) and cultured in RPMI-1640

Table 1 Cytotoxicity results with A549 (NSCLC) and BEAS-2B cell lines at 50 μM

		A549 (NSCLC)			BEAS-2B cell line		
Compounds	Conc (μM)	% cell viability	% inhibition	IC_{50} (μM) values	% Cell viability	% Inhibition	IC_{50} values
Normal (control)	—	100	0	—	100	0	—
Cisplatin CP (standard)	50	25.49	72.91	23.2 ± 0.7	76.23	23.16	>40
HA/Fe-MOF/CP	50	19.73	82.72	17.3 ± 0.5	85.34	17.23	>40
Fe-MOF/CP	50	21.87	76.42	22.4 ± 0.3	79.98	18.94	>40
Fe-MOF	50	39.53	60.41	35.6 ± 0.5	89.31	12.12	>40

medium supplemented with 10% fetal bovine serum, 1% penicillin–streptomycin, and 2 mM L-glutamine at 37 °C in a humidified atmosphere containing 5% CO_2. Following a 24-hour period, the cell culture medium was removed, and varying concentrations of the test materials (7.81–500 μM) dissolved in culture medium were delivered to the cells, which were then incubated for an additional 48 h. After incubation, 10 μL of MTT (12 mM) reagent was introduced to each well, and the cells were incubated for an additional 4 hours. After incubation, the medium was discarded, and 100 μL of DMSO was introduced to each well to dissolve the formazan crystals. The absorbance at 570 nm was measured using a PerkinElmer EnSpire 2300 multimode reader. The studies were carried out in triplicate, and the final results were calculated as the average of three trials. A nonlinear regression model in GraphPad Prism 8 was used to determine the IC_{50} values.

2.13 Statistical analysis

The statistical analysis for this study was carried out using GraphPad Prism 8.0. Results of the MTT experiments are shown as mean ± standard deviation. The Kruskal–Wallis test and Dunn's multiple comparison analysis were employed to determine whether group differences were statistically significant. The treatment groups' significance levels relative to the control are indicated as $^{****}p \leq 0.0001$, $^{***}p \leq 0.001$, $^{*}p \leq 0.01$, and $^{**}p \leq 0.05$.

3. Results and discussion

By using XRD analysis, the phase purity and successful synthesis of the fabricated catalysts were confirmed. As shown in Fig. 1(a), Fe-MOF displays distinct diffraction peaks at 2θ = 11.6°, 15.9°, 17.6°, 21.5°, 22.4°, 22.8°, 25.1°, 27.1°, 29.2°, 30.02°, 32.02°, 35.4°, 37.5°, 40.5°, and 48.87°, which indicate a well-defined crystalline framework. The decrease in intensity, slight shifting, or disappearance of several peaks following the addition of cisplatin (CP) confirmed the drug's effective encapsulation within the MOF structure. The Fe-MOF/CP composite retains major diffraction peaks at 2θ = 11.6°, 17.7°, 21.5°, 22.5°, 25.2°, 27.1°, 29.3°, 32.1°, 35.5°, 38.1°, 40.3°, and 48.9°, demonstrating that the crystalline structure remains largely preserved. The addition of hyaluronic acid (HA) shows effective absorption into the Fe-MOF framework with maxima at 2θ = 7.1°, 10.4°, 18.5°, and 23.9°. While the HA/Fe-MOF/CP exhibits new and slightly displaced peaks at 2θ = 7.01°, 10.5°, 15.4°, 19.01°, 20.01°, 23.7°, and 28.6°, which indicate changes in the lattice structure while maintaining phase purity. The observed peak shifts and intensity decreases are consistent with drug-MOF interactions, specifically HA and Fe-MOF/CP. The

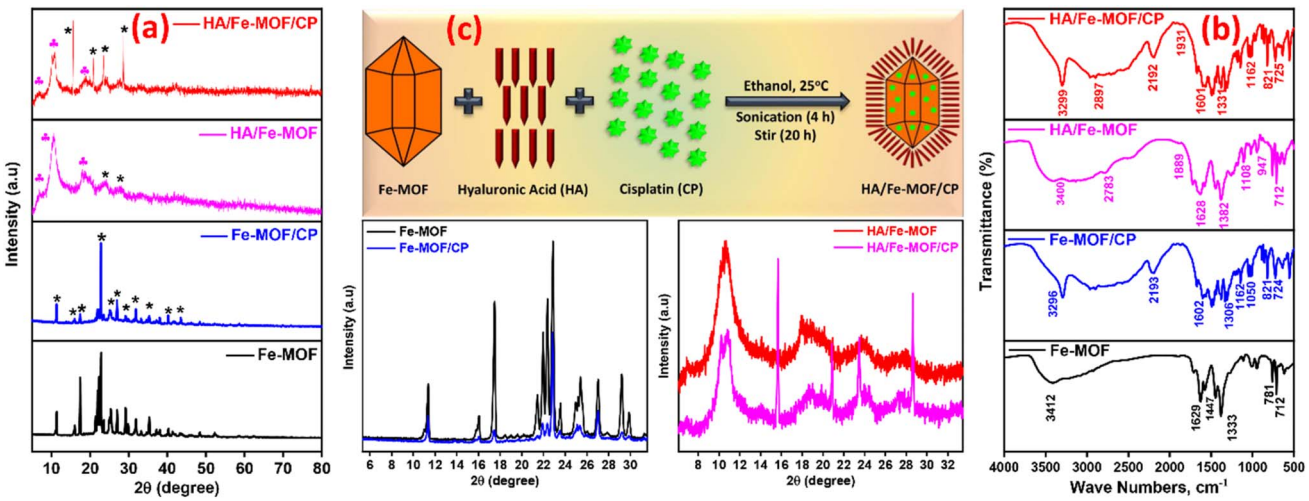

Fig. 1 (a) XRD spectra of Fe-MOF, Fe-MOF/CP, HA/Fe-MOF and HA/Fe-MOF/CP also add their magnified view. (b) FTIR spectra of Fe-MOF, Fe-MOF/CP, HA/Fe-MOF and HA/Fe-MOF/CP. (c) Reaction mechanism of HA/Fe-MOF/CP.

average crystallite sizes, calculated using the Debye–Scherrer equation, were 68.35 nm for Fe-MOF, 43.14 nm for Fe-MOF/CP, and 32.5 nm for HA/Fe-MOF/CP, indicating that functionalization and drug loading decrease particle size while enhancing structural compactness.

$$D = K\lambda/\beta \cos\theta \quad (5)$$

where θ denotes the diffraction angle, λ is the X-ray wavelength, and the variable β represents the full width at half maximum (FWHM) of the diffraction peaks. Fe-MOF's porosity and crystallinity are altered by the addition of cisplatin (CP) and hyaluronic acid (HA), which influence the drug release behaviour. Structural alterations brought about by the drug's integration into the altered framework decrease crystallinity and encourage slower, more regulated drug release. Because the framework permits slow drug diffusion, these modifications enable a sustained drug release. These structural changes are supported by the decreases in peak intensity and minor changes in peak locations, as depicted in Fig. 1(a).

Hyaluronic acid (HA) and the metal–organic framework (MOF) combine with ethanol to generate the stable HA/Fe-MOF complex. This complex forms the multifunctional structure HA/Fe-MOF/CP by efficiently binding with the chemotherapeutic agent cisplatin (CP).

The Fourier-transform infrared (FTIR) spectra of Fe-MOF, Fe-MOF/CP, HA/Fe-MOF, and HA/Fe-MOF/CP composites, which are displayed in Fig. 1(b), reveal how drug encapsulation and surface functionalization affect the structural and functional characteristics of these materials. O–H stretching vibrations from surface hydroxyl groups are responsible for the large absorption band at 3412 cm^{-1} in the FTIR spectra of pristine Fe-MOF.[28] The C=O stretching vibrations of the carboxyl groups of the organic linker are represented by the peak at 1692 cm^{-1}, while the bands at 1133 cm^{-1} and 784–712 cm^{-1} are associated with C–O and Fe–O stretching vibrations, respectively, suggesting coordination between Fe^{3+} ions and the carboxylate ligands.[29] Additional peaks at 2396 cm^{-1} and 2196 cm^{-1} in the Fe-MOF/CP spectra are recognised as N–H and C≡C stretching vibrations from the cisplatin molecule, respectively, indicating that it was successfully encapsulated within the Fe-MOF framework. The FTIR spectrum of Fe-MOF/HA displays a broadening of the O–H band at 3400 cm^{-1} and introduces a C–H stretching vibration at 2738 cm^{-1}, characteristic of hyaluronic acid (HA), along with bands at 1628 cm^{-1} (asymmetric $-COO^-$ stretching) and 1108 cm^{-1} (C–O–C and C–O stretching), signifying successful surface functionalization with HA.[30] For the HA/Fe-MOF/CP, peaks appear at 3299 cm^{-1} (O–H/N–H stretching), 2897 cm^{-1} (C–H stretching), 2192 cm^{-1} (C≡C stretching), and 1601 cm^{-1} (C=O stretching), while a peak for the Fe–O vibration is observed at 827 cm^{-1}.[31] These peaks show slight shifts and intensity changes compared to pristine Fe-MOF, reflecting strong coordination and hydrogen-bonding interactions between Fe–O, C=O, and N–H functional groups. This suggests the successful synthesis of Fe-MOF, modification with HA, and encapsulation of cisplatin within the framework.[32]

Fig. 2 presents the high-resolution XPS spectra of the HA/Fe-MOF/CP composite. Fig. 2(a) shows the C 1s peak, which can be deconvoluted into three components: C=C/C–C (284.7 eV), C–

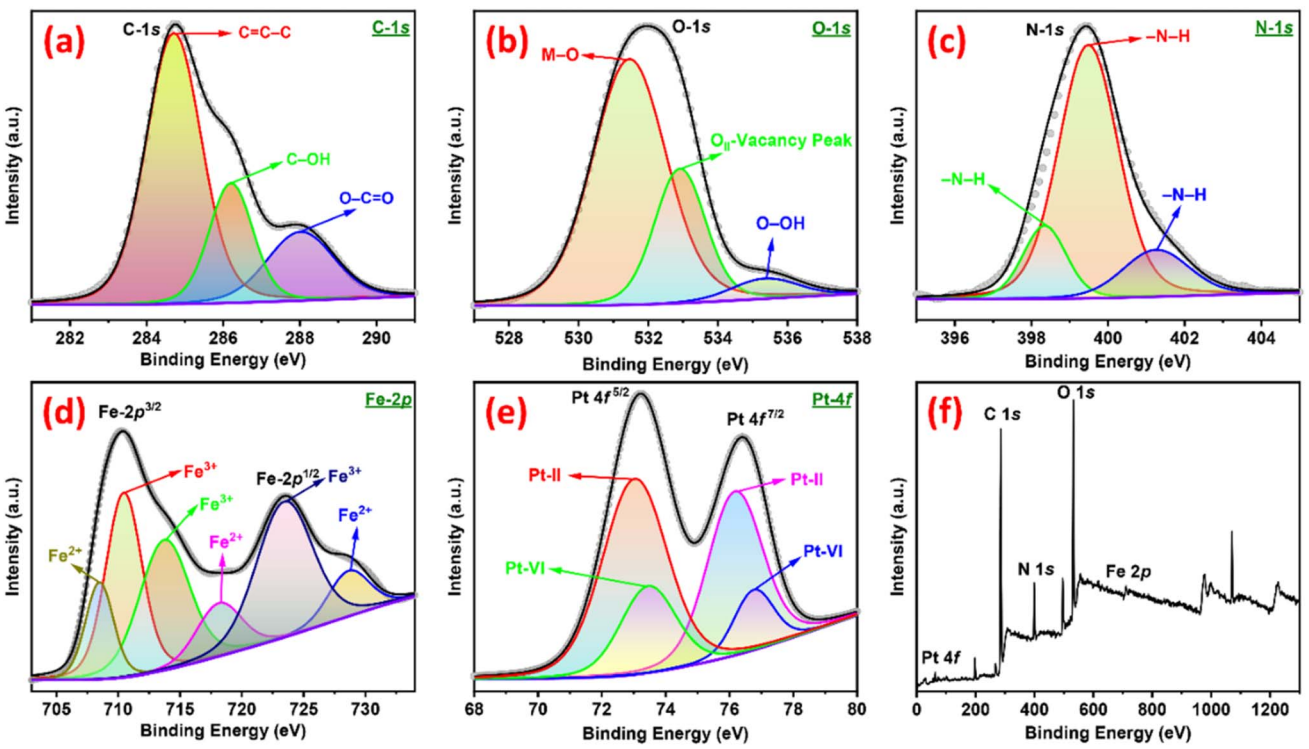

Fig. 2 XPS spectra of (a) C, (b) O, (c) N, (d) Fe and (e) Pt, and (f) the survey spectrum of HA/Fe-MOF/CP.

OH (286.2 eV), and C–O/C=O (288.2 eV). After hydroxylation, the C=O groups remained mostly unchanged, while the C–OH content increased significantly. Fig. 2(b) shows the broad O 1s peak, consisting of several components, including M-O at 531.5 eV, an OII vacancy peak at 532.9 eV, and O–OH at 535.3 eV. Fig. 2(c) shows the N 1s spectrum, which reveals a peak at 399.5 eV corresponding to pyridinic nitrogen, associated with nitrogen bonded to two carbon atoms. Additional components at 398.3 eV, 399.5 eV, and 401.2 eV are attributed to –N–H bonds.[33] Fig. 2(d) shows the Fe $2p^{3/2}$ peak at 710.3 eV, indicating the presence of Fe^{3+} in the composite. The XPS spectra of different samples reveal a transformation from Fe^{3+} to Fe^{2+}, with Fe^{3+} peaks at 710.6 eV, 713.7 eV, and 723.6 eV diminishing, while Fe^{2+} peaks at 708.4 eV, 718.4 eV, and 728.8 eV increase. The existence of Fe^0 is indicated by a minor peak at 708.4 eV.[34] Two pairs of overlapping Lorentzian curves, representing Pt $4f^{7/2}$ and Pt $4f^{5/2}$ lines at 76.4 eV and 73.2 eV, respectively, are shown in Fig. 2(e) of the Pt 4f spectrum. Peaks representing Pt-II (at 73.05 eV and 76.2 eV) and Pt-VI (at 73.4 eV and 76.8 eV) oxidation states of platinum are also present. The XPS survey spectrum, shown in Fig. 2(f), displays the distinctive peaks for carbon (C), nitrogen (N), oxygen (O), iron (Fe), and platinum (Pt).[35] The unique binding energies of these peaks confirm that each element was successfully incorporated into the HA/Fe-MOF/CP. The successful integration of platinum-based drug molecules and hyaluronic acid is confirmed by the changes in binding energies, particularly the reduction of Fe^{3+} to Fe^{2+} and the modification of nitrogen, oxygen, and platinum components. The existence of platinum in two different oxidation states (Pt-II and Pt-VI) and the change of Fe^{3+} to Fe^{2+} indicate that the composite have the potential for burst release, in which the interaction of metal ions with platinum results in a regulated and quick release of drugs.

The structural and surface modifications of Fe-MOF, Fe-MOF/CP, HA/Fe-MOF, and HA/Fe-MOF/CP caused by drug loading and functionalization are demonstrated by SEM images, histograms, and surface plots. Fe-MOF is efficient for drug-delivery applications because of its octahedral shape, which increases its surface area, as seen at 200 00x magnification in Fig. 3(a). Fe-MOF loaded with cisplatin (CP) is shown in Fig. 3(b), where the surface becomes more aggregated and rougher. The crystalline structure is further refined by functionalization with hyaluronic acid (HA) to generate HA/Fe-MOF, as shown in Fig. 3(c). In HA/Fe-MOF/CP, as depicted in Fig. 3(d),

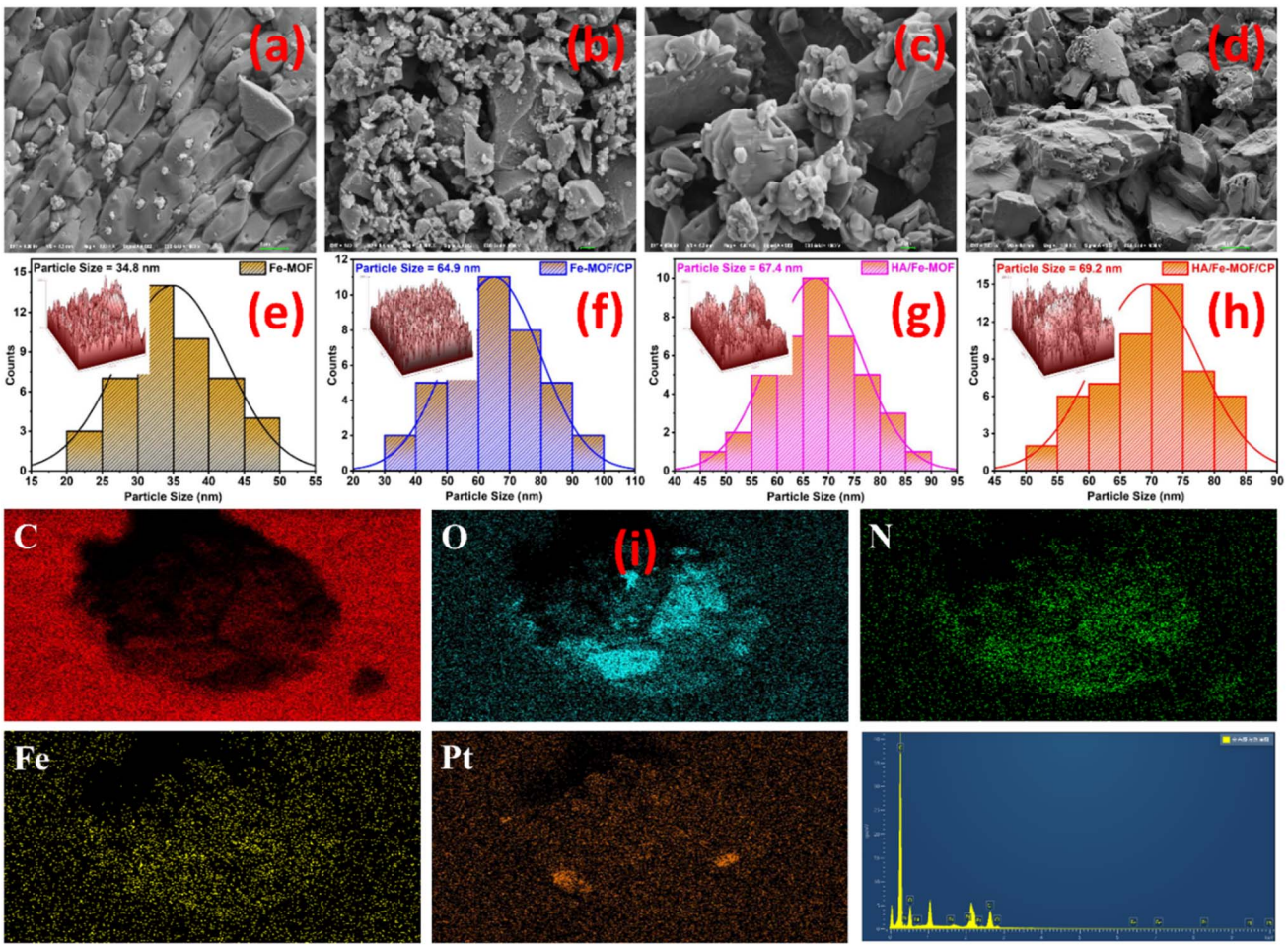

Fig. 3 SEM images of (a) Fe-MOF, (b) Fe-MOF/CP, (c) HA/Fe-MOF and (d) HA/Fe-MOF/CP. Particle size histograms and surface plots of (e) Fe-MOF, (f) Fe-MOF/CP, (g) HA/Fe-MOF and (h) HA/Fe-MOF/CP, and (i) elemental mappings and EDX spectra of HA/Fe-MOF/CP.

the drug and hyaluronic acid (HA) combination improves interaction with biological materials, enabling more efficient and regulated drug administration. The surface changes with each modification stage for Fe-MOF are shown by surface plots and histograms. Fe-MOF, as shown in Fig. 3(e), has a smooth, porous surface with an average particle size of 34.8 nm. Following the loading of cisplatin, as shown in Fig. 3(f), the surface becomes rougher and more aggregated and exhibits a wider size distribution at 64.9 nm. Furthermore, functionalization with HA increases the particle size to 67.4 nm, as shown in Fig. 3(g), improving its surface complexity and biocompatibility. The final composite, HA/Fe-MOF/CP, optimizes the material for enhanced biological interactions and effective drug administration, with the largest particle size of 69.2 nm and a highly irregular surface, as seen in Fig. 3(h). The EDX spectrum and elemental mapping displayed in Fig. 3(i) provide the material composition of the HA/Fe-MOF/CP composite. Here, the uniform distribution of carbon (C) across the sample indicates the presence of organic material. Oxygen and nitrogen signals in the EDX spectrum originate from the organic linkers of the MOF framework and from the drug components incorporated into the composite. The localized iron (Fe) indicates the iron-based components, which point to the metal–organic framework (MOF). It is confirmed that platinum (Pt) is a component of the medication structure. These conclusions are further supported by the EDX spectrum, which shows characteristic peaks for C, O, N, Fe, and Pt, along with their corresponding intensities, which reflect the relative abundances of these elements in the HA/Fe-MOF/CP.

The DLS results in Fig. 4(a and b) show a wide particle size distribution, with an average size of 2426 nm and the bulk of particles centred at 571.6 nm, indicating the presence of bigger aggregates or clusters in the material. The relatively high polydispersity index (PDI) of 0.981 implies some variability in particle size and suggests partial aggregation in suspension, which arises from nanoparticle clustering during measurement. However, TEM/SEM analysis confirms uniform morphology and nanoscale size distribution, indicating that primary particle formation is well controlled. The zeta potential of 3.26 mV shows the stability of the materials, though the low value implies a higher stability of aggregation. The zeta potential is relatively low, and the presence of hyaluronic acid provides steric stabilization and enhances biological interactions, which can compensate for electrostatic instability and support effective drug delivery performance. The HRTEM images shown in Fig. 4(c–e) reveal that the composite exhibits a nanostructured, crystalline structure with well-defined lattice spacings of 0.311 nm, reflecting high crystallinity and robust structural integrity. The uniformity of the crystalline domains of the SAED pattern emphasizes the material's high degree of order. In Fig. 4(f), lattice fingers demonstrate a periodicity consistent with the crystalline nature observed in the HRTEM images. The HA/Fe-MOF/CP composite thus exhibits outstanding crystallinity, structural stability, a broad particle size distribution and effectiveness in drug delivery.

3.1 Drug loading and release

UV-visible analysis, shown in Fig. 5(a), confirmed the successful encapsulation of cisplatin (CP) within the nanocarrier system. The spectrum of HA/Fe-MOF/CP showed a significant decrease and broadening of the characteristic cisplatin peaks compared

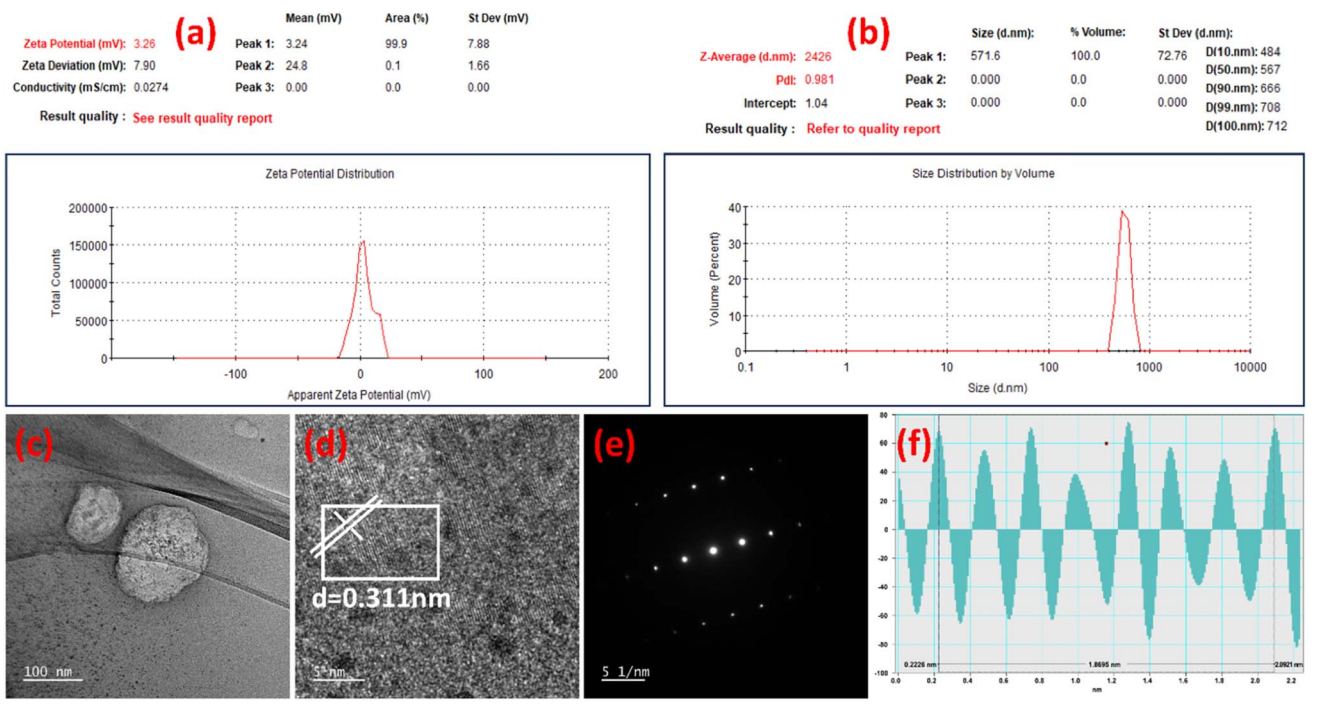

Fig. 4 (a) Zeta potential and (b) DLS Z-average size. HRTEM images at (c) 100 nm and (d) 5 nm and the *d*-spacing. (e) HRTEM SAED pattern at 5–1 nm and (f) latice fringe profile of the HA/Fe-MOF/CP.

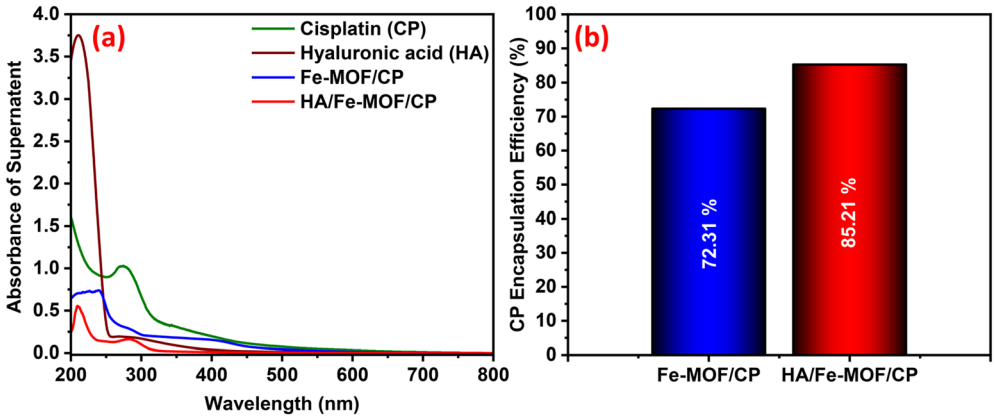

Fig. 5 (a) UV-visible spectra of cisplatin (CP), hyaluronic acid (HA), Fe-MOF/CP, and HA/Fe-MOF/CP. (b) Encapsulation efficiency of Fe-MOF/CP and HA/Fe-MOF/CP.

to the free drug. This dilution indicates that CP is effectively shielded within the Fe-MOF pores as a result of strong drug–carrier interactions. These interactions primarily involve coordination bonding between the platinum atom of cisplatin and the unsaturated iron sites (Fe-nodes) of the MOF. Hydrogen bonding stabilizes the drug within the framework. The role of hyaluronic acid (HA) is also significant. The greater reduction in the absorbance of the HA/Fe-MOF/CP spectrum demonstrates increased drug entrapment compared to Fe-MOF/CP. This is due to the functional groups of HA (–COOH, –OH), which provide additional hydrogen bonding and electrostatic interactions with CP, creating networks around the drug. Fig. 5(b) spectral evidence directly correlates with the superior encapsulation efficiency (EE%) of 85.21% for HA/Fe-MOF/CP, significantly higher than 72.31% for Fe-MOF/CP. This confirms that the multi-model bonding Fe coordination, hydrogen bonding, and electrostatic forces in the HA-coated system are responsible for the higher drug loading and improved formulation stability, and its potential for sustained drug release.

Fig. 6 illustrates the pH-responsive cisplatin release behavior of Fe-MOF/CP and HA/Fe-MOF/CP over 70 h to 270 h, convincingly demonstrating the superior tumor-selective delivery capability of the HA-functionalized system. Fig. 6(a) presents the cumulative release in the acidic tumor microenvironment (pH 5), with HA/Fe-MOF/CP exhibiting the most rapid and extensive release, reaching approximately 73.3% to 81.5% within 70 h to 270 h, respectively, significantly outperforming the drug release of 52% to 59.6% for uncoated Fe-MOF/CP. In contrast, under physiological conditions (pH 7.4), HA/Fe-MOF/CP exhibits a release of 34.5–44.2%, which is higher than that of Fe-MOF/CP (32.7–38.9%). Fig. 6(b) shows a clear bar-graph comparison, highlighting that HA functionalization reduces undesired drug release to 44.2% at pH 7.4 while simultaneously boosting on-demand release by 81.5% at pH 5. Fig. 6 illustrates HA/Fe-MOF/CP as a highly tumor-activated nanocarrier that minimizes systemic exposure and off-target toxicity while maximizing therapeutic cisplatin concentrations precisely at the tumor site, representing a substantial advancement over conventional cisplatin therapy and uncoated MOF systems.

3.2 Mechanism of drug release

The targeted delivery and pH-responsive release mechanism of HA/Fe-MOF/CP is schematically depicted in Scheme 6. After

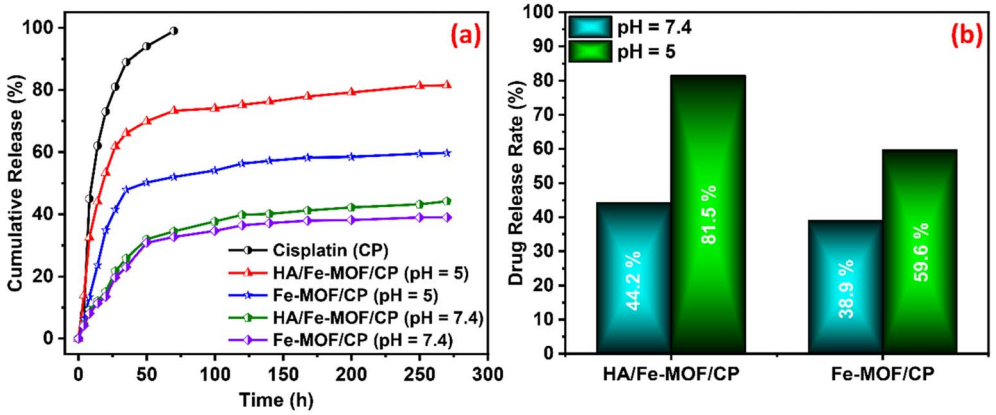

Fig. 6 (a) Cumulative release of cisplatin (CP), HA/Fe-MOF/CP and Fe-MOF/CP at pH 7.4 and pH 5. (b) Percentage drug release graphs of HA/Fe-MOF/CP and Fe-MOF/CP at pH 7.4 and pH 5.

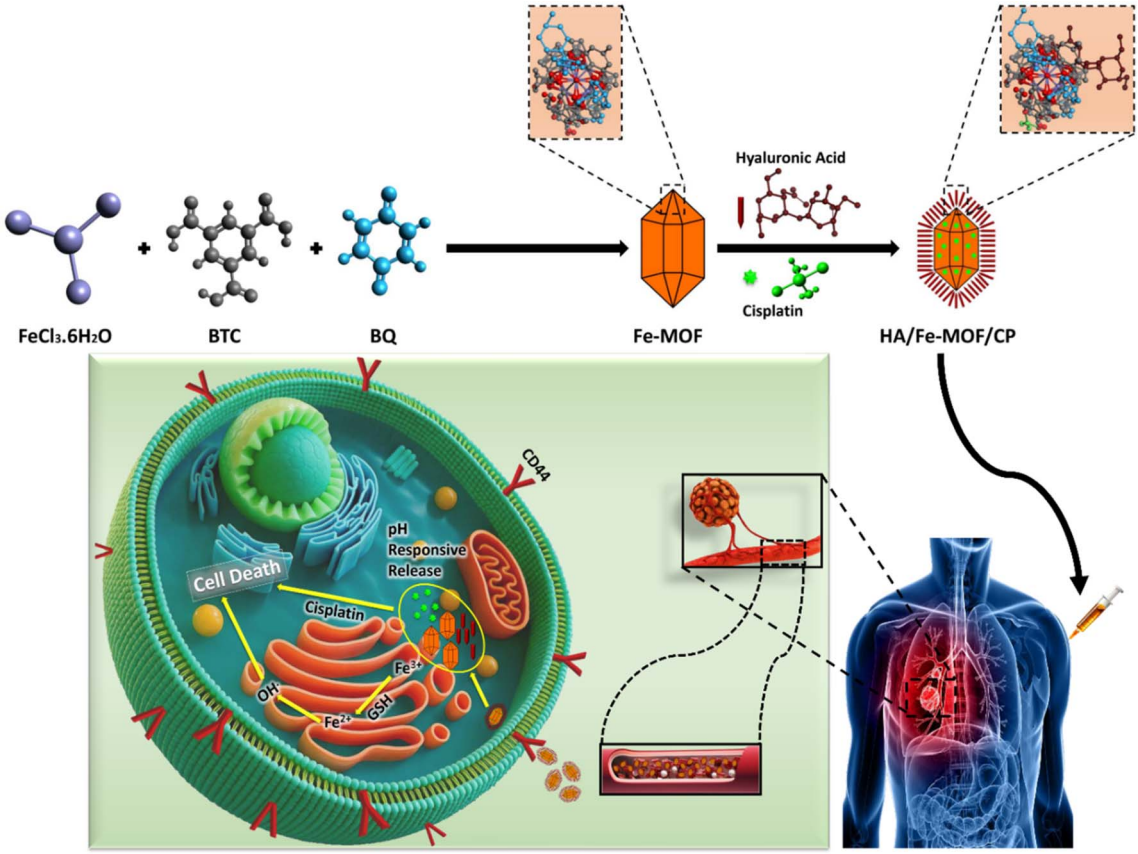

Scheme 6 Mechanism for the targeted drug delivery.

intravenous administration, the hyaluronic acid (HA) coating confers excellent colloidal stability and biocompatibility while actively targeting CD44 receptors that are highly overexpressed on A549 lung cancer cells, thereby promoting selective receptor-mediated endocytosis and enhanced intracellular accumulation of the nanocarrier. Under the neutral pH of blood circulation and healthy tissues (pH 7.4), the HA layer remains compact, and the Fe-MOF maintains structural integrity through strong Fe^{3+} carboxylate coordination bonds, effectively sealing the encapsulated cisplatin and restricting premature release to 34.5% over 70 h. However, upon reaching the acidic tumor microenvironment (pH 5) following internalization into endo/lysosomal compartments (pH 4.5–5.5), protonation of the BTC linker's carboxylate groups weakens the coordination bonds, H^+ ions competitively displace cisplatin from open Fe^{3+} sites, and the HA shell undergoes protonation-induced swelling and increased solubility, collectively triggering rapid framework destabilization and burst release of cisplatin (approximately 73.3% within 70 h). The released cisplatin then diffuses into the nucleus, forming DNA-platinum, which inhibits DNA replication and transcription and eventually promotes apoptosis in lung cancer cells. The Fe^{3+} ions are released and enter the labile iron pool following intracellular degradation of the MOF. Within the reductive cellular environment, endogenous reducing agents such as glutathione (GSH) convert Fe^{3+} to Fe^{2+}, which partially depletes cellular antioxidants. The generated Fe^{2+} catalyzes Fenton reactions with intracellular hydrogen peroxide, producing reactive oxygen species (ROS) that initiate lipid peroxidation and weaken antioxidant defenses, ultimately leading to ferroptotic cell death. This synergistic combination of CD44-mediated active targeting and precise pH-gated drug

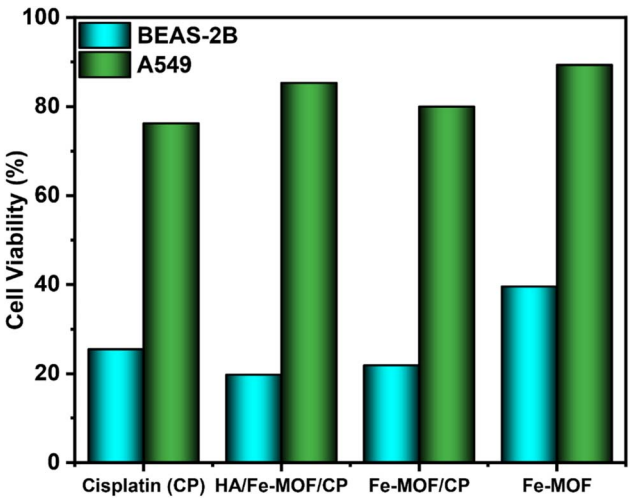

Fig. 7 *In vitro* cell viability of A549 (NSCLC) and BEAS-2B cells after 24 h incubation at 37 °C in 5% CO_2 with cisplatin (CP), HA/Fe-MOF/CP, Fe-MOF/CP and Fe-MOF at a concentration of 40 μM.

Table 2 Comparison table of the present work with previously reported studies

S. no.	Compounds	Drug loading capacity (%)	Stimulus	Drug release (%)	Time (h)	Ref.
1	HA/α-TOS@ZIF-8	43.03	pH	74 at pH 5	25	36
2	NH_2-MIL-101(Fe)@GO (luteolin and matrine)	9.8 and 14.1	pH	60.8 and 54.8 at pH 5	72	23
3	DOX@Fe-MOF@PEM	88.4	pH	72 at pH 5	12	37
4	RSSR@DOX@PEG-Gox	61.02	pH/GSH	82.1 at pH 5	48	38
5	Fe_3O_4@C@MIL-88-DOX-FC	83.6% EE, 8.3% DLC	pH	70.3 at pH 5	72	39
6	Chitosan-coated 5-fluorouracil-GEM@MIL-100	23.2	pH	77 at pH 5	48	40
7	HA/MIL-100@DOX (DMH NPs)	28	pH	66 at pH 5.5	60	41
8	MIL-100(Fe)/FA@PG	36.64	pH	73 at pH 5.5	24	42
9	P@F-FD (Fe-MIL-53-NH_2@5-FAM)	12.13	pH	81 at pH 5.5	72	43
10	**HA/Fe-MOF/CP**	**85.21**	**pH**	**85 at pH 5**	**72**	**This work**

release maximizes therapeutic efficacy at the tumor site while significantly reducing systemic toxicity, establishing HA/Fe-MOF/CP as a highly intelligent and tumor-specific cisplatin delivery platform.

3.3 *In Vitro* cytotoxicity study

After a 24-hour incubation period at 37 °C with 5% CO_2, the anticancer activity and biocompatibility of free cisplatin (CP), bare Fe-MOF, Fe-MOF/CP, and HA/Fe-MOF/CP against A549 human lung cells and BEAS-2B normal lung epithelial cells were evaluated using the MTT test. According to Table 1, free cisplatin (CP) showed significant cytotoxicity against A549 cells, exhibiting a 72.91% inhibition at 50 μM ($IC_{50} = 23.2 \pm 0.7$ μM). However, it also demonstrated a lack of selectivity by significantly harming BEAS-2B normal cells (23.16% inhibition, $IC_{50} >$ 40 μM). The targeted HA/Fe-MOF/CP nanoplatform showed the highest anticancer activity against A549 cells (82.72% inhibition at 50 μM, $IC_{50} = 17.3 \pm 0.5$ μM), indicating a significantly improved therapeutic index, while it showed significantly lower toxicity toward BEAS-2B cells (85.34% viability, 17.23% inhibition, $IC_{50} >$ 40 μM). The uncoated Fe-MOF/CP displayed intermediate efficacy, with 76.42% inhibition in A549 cells at 50 μM ($IC_{50} = 22.4 \pm 0.3$ μM), and moderate toxicity toward BEAS-2B cells (79.98% viability, $IC_{50} >$ 40 μM). The inherent safety of the Fe-MOF was confirmed by the fact that pristine Fe-MOF showed the lowest cytotoxicity against cancer cells (60.41% inhibition, $IC_{50} = 35.6 \pm 0.5$ μM) but the highest biocompatibility, with 89.31% cell viability in BEAS-2B cells are shown in Fig. 7. The gradual improvement from Fe-MOF, Fe-MOF/CP, to HA/Fe-MOF/CP makes it abundantly evident that cisplatin encapsulation and hyaluronic acid functionalization work in concert to increase anticancer potency and selectivity. This improvement is accomplished by pH-triggered release that only occurs within tumor cells, increased intracellular drug accumulation, and endocytosis mediated by CD44 receptors. The dose–response curves and corresponding IC_{50} values clearly demonstrate that HA/Fe-MOF/CP exhibits significantly greater cytotoxicity against cancer cells and superior compared to free cisplatin and unfunctionalized formulations across all tested concentrations, establishing it as a more effective and selective for cisplatin-based lung cancer therapy. Although we did not include receptor-blocking, uptake, or competitive binding studies in this work, the selective cytotoxicity observed toward CD44-overexpressing cancer cells, along with literature supporting HA-CD44 interactions, suggests that our system effectively targets CD44 receptors. A table for comparison with previously reported materials is given in Table 2.

4. Conclusion

The HA/Fe-MOF/CP nanoplatform showed promising results in enhancing cisplatin delivery for lung cancer therapy. The combination of hyaluronic acid modification and iron-based metal–organic framework (Fe-MOF) enabled targeted drug delivery through CD44 receptor-mediated endocytosis, significantly improving the anticancer efficacy of cisplatin. Cytotoxicity assays demonstrated that HA/Fe-MOF/CP achieved 82.72% inhibition in A549 lung cancer cells at 50 μM ($IC_{50} = 17.3 \pm 0.5$ μM), which is notably higher compared to that of free cisplatin (72.91% inhibition, $IC_{50} = 23.2 \pm 0.7$ μM). Significantly, the HA/Fe-MOF/CP nanoplatform, with 85.34% cell viability and $IC_{50} >$ 40, demonstrated less toxicity to normal BEAS-2B cells than free cisplatin, which inhibited BEAS-2B cells by 23.16% with $IC_{50} >$ 40. These results demonstrate HA/Fe-MOF/CP's improved tumor selectivity and decreased systemic toxicity, supporting its promise as a safer and more successful lung cancer treatment option than traditional cisplatin chemotherapy. This pH-responsive, targeted delivery system offers an innovative approach for overcoming the limitations of traditional chemotherapy, improving therapeutic outcomes while minimizing side effects.

Author contributions

Ammar Saleem: wrote the introduction, synthesized the materials and prepared XRD graphs. Komal Zaman Khan: authored the materials and synthesis section and conducted the experimental work. Ali Junaid: assisted with the introduction and experimental sections, wrote the results and discussion section, and preparation of XPS, DLS and zeta potential graphs. Aurang Zaib: performed cytotoxicity experiments and analyzed the graphical data. Ghazanfar Abbas: developed material structures and performed XPS and XRD analyses. Muhammad Naeem Ashiq: Prepared XPS, UV and TEM graphs and reviewed the Results and Discussion section. Eman Fayad

and Dalal Nasser Binjawhar: provided funding and characterization resources, verified the data, and provided instrumentation. Zahid Shafiq and Hua Li Qin: supervised the study, reviewed the full manuscript, and contributed to writing-review and editing.

Conflicts of interest

The authors declare no conflicts of interest.

Data availability

The data supporting this article have been included as part of the supplementary information (SI). Supplementary information is available. See DOI: https://doi.org/10.1039/d6ra00754f.

Acknowledgements

We are grateful to Wuhan University of Technology for its support. The authors extend their appreciation to the Princess Nourah bint Abdulrahman University Research Supporting Project number (PNURSP2026R155), Princess Nourah bint Abdulrahman University, Riyadh, Saudi Arabia.

References

1 A. Saini, M. Kumar, S. Bhatt, V. Saini and A. Malik, Cancer causes and treatments, *Int. J. Pharma Sci. Res.*, 2020, **11**, 3121–3134.
2 K. C. Thandra, A. Barsouk, K. Saginala, J. S. Aluru and A. Barsouk, Epidemiology of lung cancer, *Wspolczesna Onkol.*, 2021, **25**, 45–52.
3 M. B. Schabath and M. L. Cote, Cancer progress and priorities: lung cancer, *Cancer Epidemiol., Biomarkers Prev.*, 2019, **28**, 1563–1579.
4 E. Jakobsen, K. E. Olsen, M. Bliddal, M. Hornbak, G. F. Persson and A. Green, Forecasting lung cancer incidence, mortality, and prevalence to year 2030, *BMC Cancer*, 2021, **21**, 985.
5 T. Wang, R. A. Nelson, A. Bogardus and F. W. Grannis Jr, Five-year lung cancer survival: which advanced stage nonsmall cell lung cancer patients attain long-term survival?, *Cancer*, 2010, **116**, 1518–1525.
6 S. V. Mathan, M. Rajput, and R. P. Singh, Chemotherapy and radiation therapy for cancer, in *Understanding Cancer*, Elsevier, 2022, pp. 217–236.
7 P. Tagde, A. Najda, K. Nagpal, G. T. Kulkarni, M. Shah, O. Ullah, S. Balant and M. H. Rahman, Nanomedicine-based delivery strategies for breast cancer treatment and management, *Int. J. Mol. Sci.*, 2022, **23**, 2856.
8 G. Adorno and G. Brownell, Understanding quality-of-life while living with late-stage lung cancer: an exploratory study, *J Soc Work End Life Palliat Care*, 2014, **10**, 127–148.
9 S. Ingole, N. Vasdev, M. Tekade, T. Gupta, B. Pawar, M. Mhatre, A. G. Prasad, and R. K. Tekade, Toxic effects of cancer therapies, in *Public Health and Toxicology Issues in Drug Research*, Elsevier, 2024, pp. 353–379.
10 T. C. Ezike, U. S. Okpala, U. L. Onoja, C. P. Nwike, E. C. Ezeako, O. J. Okpara, C. C. Okoroafor, S. C. Eze, O. L. Kalu and E. C. Odoh, Advances in drug delivery systems, challenges and future directions, *Heliyon*, 2023, **9**, e17488.
11 Y. Sun, L. Zheng, Y. Yang, X. Qian, T. Fu, X. Li, Z. Yang, H. Yan, C. Cui and W. Tan, Metal–organic framework nanocarriers for drug delivery in biomedical applications, *Nano-Micro Lett.*, 2020, **12**, 103.
12 R. Zhu, M. Cai, T. Fu, D. Yin, H. Peng, S. Liao, Y. Du, J. Kong, J. Ni and X. Yin, Fe-based metal organic frameworks (Fe-MOFs) for bio-related applications, *Pharmaceutics*, 2023, **15**, 1599.
13 H. Yang, D. Liao, Z. Cai, Y. Zhang, A. Nezamzadeh-Ejhieh, M. Zheng, J. Liu, Z. Bai and H. Song, Current status of Fe-based MOFs in biomedical applications, *RSC Med. Chem.*, 2023, **14**, 2473–2495.
14 M. Srinivasarao and P. S. Low, Ligand-targeted drug delivery, *Chem. Rev.*, 2017, **117**, 12133–12164.
15 Y. Xu, J. Benedikt and L. Ye, Hyaluronic acid interacting molecules mediated crosstalk between cancer cells and microenvironment from primary tumour to distant metastasis, *Cancers*, 2024, **16**, 1907.
16 G. Mattheolabakis, L. Milane, A. Singh and M. M. Amiji, Hyaluronic acid targeting of CD44 for cancer therapy: from receptor biology to nanomedicine, *J. Drug Targeting*, 2015, **23**, 605–618.
17 J.-N. Hao, K. Ge, G. Chen, B. Dai and Y. Li, Strategies to engineer various nanocarrier-based hybrid catalysts for enhanced chemodynamic cancer therapy, *Chem. Soc. Rev.*, 2023, **52**, 7707–7736.
18 M. Moradi, M. Aliomrani, S. Tangestaninejad, J. Varshosaz, H. Kazemian, F. S. Emami and M. Rostami, Hyaluronic acid targeted metal organic framework based on iron (III) for delivery of platinum curcumin cytotoxic agent to triple negative breast cancer cell line, *Appl. Organomet. Chem.*, 2022, **36**, e6755.
19 J. Kryczka, J. Kryczka, K. H. Czarnecka-Chrebelska and E. Brzezińska-Lasota, Molecular mechanisms of chemoresistance induced by cisplatin in NSCLC cancer therapy, *Int. J. Mol. Sci.*, 2021, **22**, 8885.
20 Z. Zong, G. Tian, J. Wang, C. Fan, F. Yang and F. Guo, Recent advances in metal–organic-framework-based nanocarriers for controllable drug delivery and release, *Pharmaceutics*, 2022, **14**, 2790.
21 R. Ranasinghe, M. L. Mathai and A. Zulli, Cisplatin for cancer therapy and overcoming chemoresistance, *Heliyon*, 2022, **8**, e10608.
22 Z. Guo, Y. Xiao, W. Wu, M. Zhe, P. Yu, S. Shakya, Z. Li and F. Xing, Metal–organic framework-based smart stimuli-responsive drug delivery systems for cancer therapy: advances, challenges, and future perspectives, *J. Nanobiotechnol.*, 2025, **23**, 157.
23 J.-J. Shen, S.-J. Xue, Z.-H. Mei, T.-T. Li, H.-F. Li, X.-F. Zhuang and L.-M. Pan, Synthesis, characterization, and efficacy evaluation of a PH-responsive Fe-MOF@ GO composite

drug delivery system for the treating colorectal cancer, *Heliyon*, 2024, **10**, e28066.

24 P. Raju, K. Balakrishnan, M. Mishra, T. Ramasamy and S. Natarajan, Fabrication of pH responsive FU@ Eu-MOF nanoscale metal organic frameworks for lung cancer therapy, *J. Drug Delivery Sci. Technol.*, 2022, **70**, 103223.

25 A. Ahmed, A. Karami, R. Sabouni, G. A. Husseini and V. Paul, pH and ultrasound dual-responsive drug delivery system based on PEG–folate-functionalized Iron-based metal–organic framework for targeted doxorubicin delivery, *Colloids Surf., A*, 2021, **626**, 127062.

26 F. Yang, Q. Dong, Z. Chen, B. Gao, D. Zheng, R. Wang, S. Qin, F. Peng, M. Luo and J. Yang, A ph-responsive drug-delivery system based on apatinib-loaded metal-organic frameworks for ferroptosis-targeted synergistic anti-tumor therapy, *Int. J. Nanomed.*, 2024, 9055–9070.

27 Y. Hassanpouraghdam, M. Pooresmaeil and H. Namazi, In-vitro evaluation of the 5-fluorouracil loaded GQDs@ Bio-MOF capped with starch biopolymer for improved colon-specific delivery, *Int. J. Biol. Macromol.*, 2022, **221**, 256–267.

28 O. V. Enearepuadoh, I. Deborah and D. E. J. M. Dixon, Synthesis, Characterization, and Sorption study of Fe-MOF on Crude oil Remediation in Niger Delta Region of Nigeria, *Modern Physical Chemistry Research*, 2022, **2**, 1–10.

29 S. Pasieczna-Patkowska, M. Cichy and J. J. M. Flieger, Application of Fourier transform infrared (FTIR) spectroscopy in characterization of green synthesized nanoparticles, *Molecules*, 2025, **30**, 684.

30 F. Xiong, Z. Qin, H. Chen, Q. Lan, Z. Wang, N. Lan, Y. Yang, L. Zheng, J. Zhao and D. J. J. Kai, pH-responsive and hyaluronic acid-functionalized metal–organic frameworks for therapy of osteoarthritis, *J. Nanobiotechnol.*, 2020, **18**, 139.

31 H. S. Lere and G. Wyasu, Green Synthesis Of Iron And Zinc Nano Particles Using Grape Extract, *CaJoST*, 2024, **6**, 333–341.

32 W. Ji, W. Li, Y. Wang, T. C. Zhang, Y. Wei, S. J. S. Yuan and P. Technology, Zr-doped MIL-101 (Fe)/Graphene oxide nanocomposites: An efficient and water-stable MOF-based adsorbent for As (V) adsorption in aqueous solution, *Sep. Purif. Technol.*, 2024, **339**, 126681.

33 T. Susi, T. Pichler and P. Ayala, X-ray photoelectron spectroscopy of graphitic carbon nanomaterials doped with heteroatoms, *Beilstein J. Nanotechnol.*, 2015, **6**, 177–192.

34 Z. Hou, P. Yan, B. Sun, H. Elshekh and B. Yan, An excellent soft magnetic Fe/Fe3O4-FeSiAl composite with high permeability and low core loss, *Results Phys.*, 2019, **14**, 102498.

35 V. S. Alabusheva, V. V. Shilovskikh, L. A. Bridenko, V. V. Gurzhiy and E. V. Skorb, Synthesis of catalytic microswimmers based on anisotropic platinum sorption on melamine barbiturate supramolecular structures, *Adv. Intell. Syst.*, 2023, **5**, 2200436.

36 Q. Sun, H. Bi, Z. Wang, C. Li, X. Wang, J. Xu, H. Zhu, R. Zhao, F. He and S. Gai, Hyaluronic acid-targeted and pH-responsive drug delivery system based on metal-organic frameworks for efficient antitumor therapy, *Biomaterials*, 2019, **223**, 119473.

37 S. Wang, H. Wu, K. Sun, J. Hu, F. Chen, W. Liu, J. Chen, B. Sun and A. M. S. Hossain, A novel pH-responsive Fe-MOF system for enhanced cancer treatment mediated by the Fenton reaction, *New J. Chem.*, 2021, **45**, 3271–3279.

38 H. Yao, R. Ji, X. Song, B. Yang, Y. Lv and Z. Wei, A pH/GSH dual-responsive Fe-based MOF drug carrier for ferroptosis-glycolysis synergistic therapy, *New J. Chem.*, 2025, **49**, 11423–11433.

39 S. Karimi and H. Namazi, Fabrication of biocompatible magnetic maltose/MIL-88 metal–organic frameworks decorated with folic acid-chitosan for targeted and pH-responsive controlled release of doxorubicin, *Int. J. Pharm.*, 2023, **634**, 122675.

40 A. K. Resen, A. Atiroğlu, V. Atiroğlu, G. G. Eskiler, I. H. Aziz, S. Kaleli and M. Özacar, Effectiveness of 5-Fluorouracil and gemcitabine hydrochloride loaded iron-based chitosan-coated MIL-100 composite as an advanced, biocompatible, pH-sensitive and smart drug delivery system on breast cancer therapy, *Int. J. Biol. Macromol.*, 2022, **198**, 175–186.

41 T. Xue, C. Xu, Y. Wang, Y. Wang, H. Tian and Y. Zhang, Doxorubicin-loaded nanoscale metal–organic framework for tumor-targeting combined chemotherapy and chemodynamic therapy, *Biomater. Sci.*, 2019, **7**, 4615–4623.

42 F. Mokhtarian, B. Rastegari, S. Zeinali, M. Tohidi and H. R. Karbalaei-Heidari, Theranostic Effect of Folic Acid Functionalized MIL-100 (Fe) for Delivery of Prodigiosin and Simultaneous Tracking-Combating Breast Cancer, *J. Nanomater.*, 2022, **2022**, 1108865.

43 Z. Zhang, J. He, X. Yu, G. Shi, H. Hu, Q. Yin, J. Dong and L. Hao, pH-Responsive Iron-Containing Metal–Organic Framework Nanoparticle-Based MRI Delivery System for Diagnostic and Therapeutic Treatment of Pancreatic Cancer, *ACS Appl. Nano Mater.*, 2025, **8**, 15268–15277.